An investigation into flow behavior and acoustic mechanisms at the trailing edge of an airfoil

JACKSON, Beren R. and DAKKA, Sam <http://orcid.org/0000-0001-9225-761X>

An Investigation into Flow Behavior and Acoustic Mechanisms at the Trailing Edge of an Airfoil

Beren R. Jackson and Sam M. Dakka
Department of Engineering & Math, Sheffield Hallam University, Sheffield S1 1WB United Kingdom
Sam.dakka@gmx.com

Abstract

The aerodynamic and acoustic testing of a NACA0012 airfoil section was performed in an open wind tunnel, focusing on noise mechanisms at the trailing edge to identify and understand sources of noise production. The sound measurement profiles were captured by embedding microphones along the chord at various distances from the trailing edge and at different geometric angles of attack. The embedded microphones have successfully captured all noise sources due to aerodynamic flow over the NACA 0012 airfoil at the trailing edge, which included the following major peak frequencies 44 Hz, 93 Hz, 166 Hz and 332Hz. The fundamental frequency of the model tested was identified by peak frequency (166Hz). It appears that these frequencies do not deviate as the angle of attack is increased. The general trend is Strohal numbers decrease as the flow moves downstream which indicate the amount of resonance (i.e. periodic, non-random vortices) decreases further downstream, which is to be expected given the onset of turbulence. Two bands of frequencies were identified. The frequency spectra between 1 to 3kHz show a measure of far field noise energy while frequency spectra in the range 3 to 10kHz shows near field noise energy which is due to mechanisms associated with wake flow (separation).

Keywords: airfoil self-generated noise, trailing edge noise, far field noise, near field noise.

1. Introduction

Knowledge of noise sources and mechanisms of noise production at the trailing edge of an airfoil is of great importance when considering the wing design of an aircraft. This is due to increased stringent limits and regulations imposed on allowed aircraft noise, and especially noise emitted on landing approach, a considerable source of noise pollution in airport neighboring communities. Design considerations to limit or reduce noise and vibrations have wide applications, such as in wind turbine industry, airframe design, turbomachinery, ship hulls and offshore structures.

Brookes et al. [1] have defines five airfoil self-generated noise mechanisms associated with subsonic flow surrounding an airfoil. One of these mechanisms pertinent to this study is broadband noise produced due to turbulent boundary layer trailing edge, this regime is due to flow at high Reynolds numbers, the turbulent boundary layer development is maintained on most of airfoil and the generation of broadband noise is due to turbulence that is convected over the trailing edge. If the boundary layer separates, then in addition to the broadband noise we experience several tonal peaks that are superimposed on the broadband noise, these narrow peaks perhaps are due to the vortex shedding at the trailing edge associated with the flow separation.

It has been noted, Roger and Moreau [2] that attached or separated turbulent boundary layer at the trailing edge generates broadband noise, however whistles are generated due to laminar boundary disturbances. In both scenarios noise is generated due to vortical disturbances which are transformed into acoustical ones once they are convected downstream of the trailing edge this is defined as airfoil self-noise or Trailing edge-TE noise. To understand the physics behind the self-noise production phenomena which was addressed by Roger and Moreau [3] where the exposure of vortex traveled downstream by pressure gradient is balanced by induced centrifugal forces. The source of the radiated noise is due to density variation that is induced by the thermodynamic gas properties changes caused by pressure variation due to inertia. The radiated noise is further intensified downstream due to the geometrical singularity at the trailing edge as the flow is trying to adjust itself through rapid reorganization of the vortical structures.

Analytical analysis of airfoil self-noise generation followed mainly two stream of ideas, the first is of Ffowcs Williams and Hall [4]. Where the noise radiated by the vortical disturbances of the boundary layer downstream of the trailing edge is related to the vortical velocity at the trailing edge. Amiet [5] and Howe [6] introduced the second approach which relates the far field acoustic signature statistics to the aerodynamic wall pressures statistics at some point upstream of the trailing edge. Based on this methodology the surface pressure is utilized as an equivalent acoustic source, though sound is generated due to the velocity field. The second approach has been implemented successfully by Brooks and Hodgson [7] and experimental support corroboration was reported by Brooks et al. [8] and Roger and Moreau [3].

2. **Experimental apparatus and acoustics Measurements**

A physical NACA0012 airfoil model, shown in Figure 1, was fabricated comprised of several components, each requiring different manufacturing processes. The airfoil itself was made of two components, the upper surface and lower surface, and was 3-D printed using information from CAD files exported to a format based on a coordinate system, which the 3-D printer could read (they are made from a plastic material called Acrylonitrile butadiene styrene, ABS in short). This airfoil has a chord length of 297mm and a maximum thickness of 35.6mm, and includes 10 x 0.4mm diameter pin-holes for the location of interior microphones, the exact locations are documented in table 1, It is 150mm in width. Calculations based on the new chord length were made, which enabled the placement of pin holes such that they would be near enough to the trailing edge to experience the effects of turbulence. Designing the airfoil proved to be challenging given the narrow dimensioning near the trailing edge, however the ten microphones were successfully placed as near as was possible to the trailing edge whilst maintaining the external profile. The microphones used were ‘Kingstate KECG2740PBJ Electret Condenser Microphones’, which have a diameter of 6mm and a 5.5mm height, including terminal pins. The two terminals of the microphones essentially have one terminal for the signal output (the data), which were passed through a 0.1μF capacitor and 2.2kOhm resistor, and another terminal to ground the system. A single wire carried the power supply output, which fed a signal of 2.5 volts to each microphone. During the experiment in the wind tunnel, each of these wires was probed using a 2-channel ‘PicoScope’ 5203 series Oscilloscope [9], which was able to display signal data via software on a computer. The sampling rate was 40,000 samples per second.
As indicated by the model calculations, the experiment for acoustic analysis was tested at 20m/s, with a Reynolds number (based on chord) of 406849, sufficient to cause turbulence effects, and

at angles of attack of 0, 4, 8, 12, and 16 degrees. A low-pass filter was used to cut off frequencies higher than 20kHz.

3. Acoustic Data analysis:

Calculations, based on new chord length of scaled model, shows that at a free-stream velocity of 20m/s, in level flight and for the chord length of the test model, a turbulent boundary layer is likely to develop past 37% of the overall linear chord length, and so the chosen microphone pin-hole locations (shown in table 1) are sufficient to capture turbulent effects. Figure 2 shows the location of these pin-holes on the model itself. A side view, Figure 3 is also shown for clarity.

Careful analysis of the frequency spectrums, given by the plots for each individual microphone, representative spectrum is given by plots 4 to 5 for zero angle of attack, has enabled the collation of the data presented in tables 2 to 5. The frequency measurements are plotted logarithmically, as is the convention, since this enables a clearer perspective of the patterns and trends between curves. The sampling rate of the oscilloscope was 40,000Hz, although as mentioned a low pass filter was used to measure activity below 20,000Hz. 4096 samples were plotted and an averaging method was used to plot the RMS (root mean square) value of dBu. Note that the value of dBu gives a relative measure of noise to the 'unloaded' reference level of the input voltage (hence the suffix 'u').This means that the higher the pressure induced by noise, the more attenuation is applied, via the microphone, to the individual microphone's voltage supply. Essentially this information is relayed back through the data channel and hence it is the difference between *reduction* in voltage, compared to the original input, which gives a measure of relative dB between frequencies. This is also the reason that the dBu values are negative (the more negative, the less the perceived volume).

The spectra suggest some interesting developments which will be discussed in detail later, in general, the most dominant activity relating to noise contribution with regards to airflow around the *airfoil* happens in the regions between around 200- 7000Hz. It is suggested that the most revealing area for investigation into aero-acoustic noise concerned with the NACA 0012 model begins at around 500-1000Hz, when the curves become less erratic and display an interesting change in gradient towards the latter part of the spectra, which levels out again at around 10,000Hz. Since *all* of the spectra show loud (bass/low-mid) peaks at around 44, 93 and 166Hz, and a similarly less dominant peak at around 327-330Hz, it may be that these/one of these frequencies is due to the wind tunnel fan (which ran constantly at the same speed), but the majority of these peaks could also be due to surface flow phenomena entirely related to the experimental model; information from experimental sources provided during validation will make light of the reasons for such peaks. The changes in gradients observed have been plotted for closer inspection, between 1000 and 10,000Hz, for mic. no's 1, 5 & 10, Tables 6 to 9 present data from calculations of Strouhal number (see Appendix 1) for various peak frequencies. Graphs are given (see figure 10) which plot these Strouhal numbers against chord length percentage (x/c), for visual understanding of turbulence and vortex shedding phenomena.

4. Validation

Considering the complexity of the experiment, observed results have in fact correlated well with existing data – considered validation data includes the energy/frequency spectra (as

mentioned previously, the sound pressure level is effectively measure of the noise energy), the calculated values for boundary layer parameters and skin friction, and also existing data for Strouhal number calculations on similar experiments.

4.1 Energy/Frequency Spectra:

When reviewing the energy/frequency spectrums of similar experiments, it has become clear that the experiment performed in the present research has captured noise mechanisms related to the NACA 0012 airfoil to a significant level. This is demonstrated through the comparison of current results to Garcia-Sagrado, A. and Hynes, T. [10] tested for lower Reynolds numbers. Although a lower Reynolds number than the one tested presently, the results are strikingly similar. For example, there are dominant peaks in frequency at around 190Hz and also at around 380Hz – a similar observation can be made from the noise spectra, where these two early dominant peaks correspond to around 44Hz and 166Hz.

Towards the trailing edge, overall noise (or, energy) is seen to reduce, which is also what has been observed in the spectra for the present experiment, albeit scaled differently; in the region of around 200-1000Hz, a reduction in pressure level can be seen. Following the report by Garcia-Sagrado, A. and Hynes, T. [10] which included spectra for a Reynolds number of 200,000 and 400,000, with altered angles of attack of 12.6 and 16 degrees. It is interesting to note the decay of the slope in each graph; it appears that at the trailing edge, for smaller frequencies, the energy is *relatively* lower initially (than towards the leading edge), whereas past a certain point, noise energy towards the trailing edge is lost at a faster rate (most spectral plots cross paths) than at the leading edge. It also appears that for the Reynolds number of 400,000, the *total* spectral energy is higher as the angle of attack is increased from 12.6° to 16°. Excluding microphone 1 in the present experiment, the spectral plots of microphones 5 and 10 in figures 6 to 9 show just this phenomenon, which would suggest that the experiment has been successfully performed, and valid results have been obtained for the present situation.
Furthermore, it is stated that for shear noise layers, the slopes of the noise spectra decay after a "broad" peak, Lilley, [11], which varies with f^n where n = 1.5 to 2.0, since the slope decay after the peak frequency is not universal (as is observed by different airfoil positions, angles of attack and Reynolds numbers).

4.2 Boundary Layer & Skin Friction Values:

Comparing table 10, experimental data by Brooks & Hodgson [12], it can be seen that the orders of magnitude of the skin friction coefficient (at 23.2m/s free- stream velocity) are similar to those calculated and presented in table 11. At 20% chord, the laminar skin friction coefficient was calculated to be 0.00233, similar to those in table 10.

Depending on whether flow is laminar or turbulent, the boundary layer thickness was calculated to be within around 1-8mm (0.1-0.8cm), a similar order of magnitude to the displacement thickness given in table 10 by Brooks & Hodgson; due to the fact that the velocity increases asymptotically from the airfoil surface up until reaching free-stream velocity, displacement thickness (δ^*) is effectively a measure of boundary layer thickness, but scaled as if the flow were inviscid, Banks [13] Also, as the speed is increased (represented by the Reynolds number in table 11), the value of skin friction coefficient decreases, as is observed in table 11. Thus the recorded data for the present experiment appear to be valid.

4.3 Strouhal Values:

Figures 11 and 12 show plot points of peak frequency Strouhal numbers calculated in experiments by Brooks, Pope and Marcolini [1], using a NACA 0012 airfoil, with the minimum

tested speed being 31.7m/s, and with angles of attack of between 0° to 25.2°. Figure 11 gives the plots for a laminar boundary layer whereas figure 12 gives the plots for a turbulent boundary layer. Although the data are for a slightly higher speed, it is clear that the Strouhal numbers calculated for various peak frequencies (tables 6 to 9) would fit within the same magnitude. For a laminar boundary layer, the peak Strouhal numbers appear to lie within around 0.18 to 0.3, whereas they lie within 0.04 to 0.5 for a turbulent boundary layer. In general, for a laminar boundary layer they also appear to decrease in magnitude with angle of attack, whereas under a turbulent boundary layer the Strouhal numbers increase in magnitude with angle of attack. Looking at the plotted Strouhal numbers in figures 10(a) to 10(g), this would suggest that along some parts of the airfoil there may be re-laminarisation of the turbulent boundary layer, however the Strouhal numbers do show this trend in figure 10(e) (peak frequency 5) and figure 10(f) (Strouhal number averages) at the airfoil chord length (x/c) of about 0.84 onwards.

Since many calculations have been performed for each microphone and at each angle of attack, a lot of data has been collected (much is given in tables 6 to 13); for conciseness, example calculations are given in Appendix 1 for data at 20% chord (x/c = 0.2), and microphones 1, 5 and 10. In the case of Strouhal numbers, example calculations are given for peak frequency 5 at 16° AoA, and for microphones 1, 5 and 10. Tables 11 to 13 summarize the data for all points.

5. Results

Firstly, looking at tables 8 to 11, it is interesting to note that the first four peak frequencies do not deviate significantly between measurements at each angle of attack (they are 44, 93, 166 and 332Hz approximately). It was at first thought that these peaks may have been related to the mechanisms of the wind tunnel fan, however, given that these results are very similar in form to those reported by Garcia-Sagrado and Hynes [14] (of whom included measures to reduce fan noise), it is suggested that these peak frequencies arise due to the generation of vortical structures such as described in the introduction. A revealing observation is the fact that, using the wave equation to determine the second harmonic of the frequency peak at 166Hz in fact gives a value of 332Hz (peak frequency 4), whereas the first, fifth and 'knee' frequencies are not related harmonically, and so must be related to the behaviour of the flow itself, or due to shear interactions between the flow and the airfoil surface. Thus it can be deduced that the embedded microphones have successfully captured all noise sources due to aerodynamic flow over the NACA 0012 airfoil at the trailing edge – and the fundamental frequency of the model is therefore given by peak frequency 3 (166Hz). Since the second harmonic frequency of the fundamental frequency has been identified, which appears to reduce in energy as angle of attack is increased as revealed by the noise spectrums plots; this could be explained by the initial propagation of Tollmien- Schlichtin waves, the initial wavelength of which is determined by the fundamental/natural frequency at which the NACA 0012 model resonates at. This is therefore an indication of laminar-boundary-layer vortex shedding noise. Further downstream, the second harmonic is less pronounced, and so it can be inferred that the Tollmien-Schlichting waves have become much more unstable, and consequentially, other noise mechanisms dominate, which must relate more to turbulent trailing edge noise.

At this point, much can be inferred from the gradients of the frequency spectra in the range of around 1-10kHz, as presented in figures 6 to 9 (for microphones 1, 5 and 10). Some particularly telling observations are the steepening of the slope with increase in angle of attack for microphone 1, and also the decay of the slopes of microphones 5 and 10. These observations could also be related to the steepening and magnitude of the adverse pressure gradient, and would suggest that for a given point (or microphone location), for different angles of attack, vortices are at different stages of development. Since there is more turbulence within the boundary layer at the same chord-wise point for an increased angle of attack, it is posited that the shape and gradient of the slopes given in figures 6 to 9 is determined by the onset of Kelvin-Helmholtz instabilities.

This is because, at lower angles of attack, for the same location, a higher proportion of higher

frequencies are observed than at higher angles of attack, since the Kelvin- Helmholtz instabilities have had less time to dissipate, and therefore vortices are smaller at such a point, and therefore shorter wavelengths (and hence higher frequencies) are observed. This theory is further supported by the fact that plotted Strouhal numbers (see figure 10) appear to have significant variation at the higher frequencies of peak frequency five and also at the knee frequency, which is the frequency measured at the point just before the slope begins to decay linearly, as compared to for example, peak frequencies three and four. This means that there are more inherent turbulent mechanisms at these frequencies (such as the mixing of flow due to Kelvin-Helmholtz instabilities), but at the same time, the general trend is for the Strouhal number to decrease as flow moves further downstream, meaning that the amount of resonance (i.e. periodic, non-random vortices) decreases further downstream, which is to be expected given the onset of turbulence.

Another interesting observation (figures 6 to 9) is the fact that the sound pressure level at microphone 10 appears to decay sooner than microphone 5, within the region of 3-10kHz, yet is still always significantly higher in magnitude to microphone 1. This decay of microphone 10 seems to come closer to replicating that of microphone 5, as angle of attack is increased, yet, looking closely at the frequency range 1-3kHz, the increase in sound pressure level of microphone 10 over microphone 5 can be seen. Essentially, there is a crossover point between these regions which appears to happen earlier, as angle of attack is increased. Since it has been established that Kelvin-Helmholtz instabilities are thought to play a key role in the profile of these gradients, this would suggest that there is in fact a higher amount of turbulent energy at microphone 5 in the region of about 3-10kHz, than there is at microphone 10, for lower angles of attack. Consider that microphone 1 could always be in a region which experiences similar, viscous flow behavior (less unstable), whereas if the flow is more turbulent downstream at microphone 5 and 10, it would make sense to observe a higher proportion of higher frequencies, which is the case. When the frequencies are broken down further into the bands between 1-3kHz, and 3-10kHz however, further hypotheses can be made.

Between 1-3kHz, a suggestion is that the frequency spectra show a measure of the far-field noise energy; microphone 1 measures less energy in this portion because the boundary layer is still relatively small, effectively it may be measuring the free-stream flow energy outside of the boundary layer, whereas microphone 5 and 10 are actually measuring energy *within* the boundary layer, which has grown to a sufficient size at this point, and where microphone 5 detects the turbulent energy slightly closer to the outer edge of the boundary layer than does microphone 10, which measures a higher turbulent energy.

On the other hand, between 3-10kHz, a phenomenon which would explain the differences in slope at microphones 5 and 10 is separation stall noise; as angle of attack is increased, the boundary layer at microphone 10 has a much higher affinity to separate (higher local Reynolds number) than microphone 5 (and microphone 1), therefore within the near-field region there is less energy due to small-scale vortical formations than there is at microphone 5, and effectively the only noise energy being measured is due to the back-draft of wake flow, which would also explain why the slope of microphone 10 becomes closer to microphone 5 as angle of attack is increased, since microphone 5 is also beginning to detect noise mechanisms due to wake flow. This theory is also supported by the calculations of boundary layer thickness, skin friction and wall shear stress (see table 11), which show that viscous forces do in fact reduce with location along the trailing edge.

As previously mentioned, a probable source of error in the acoustic testing was considered to be the fan blades which drive the wind tunnel, however as this source has been deemed insignificant with relation to the actual shape of the energy/frequency spectra, the only deviation of measurements due to this source could be the overall magnitude of the sound

pressure level, but given that the most important factor in determining how noise phenomena interact at the trailing edge is the shape and characteristic peaks of the spectra, and how they relate at each angle of attack, this potential source of error is largely irrelevant, since the research set out to understand noise mechanisms, first and foremost, rather than deriving a universal sound level, this potential source of error is largely irrelevant, this is no major issue.

Another source of error which may have affected the results portrayed by the acoustic testing, is the surface roughness of the airfoil model; since validation data of similar experiments such as by Garcia-Sagrado and Hynes [14] used an airfoil with a very smooth surface, whereas due to the limits of the 3-D printing mechanism used, the produced airfoil model had a slightly higher surface roughness, which would explain why the spectra given as validation data appear to decay sooner (or at least with steeper gradient), as there is less near-field turbulence associated with the surface roughness.

A final source of error is the fact that the microphones used have their own frequency response, which is inevitably slightly different to the frequency response of the microphones used in similar experiments. However, this response only affects results past 10kHz, which was considered during testing, and hence why measurements were plotted up to 10kHz.

6. Conclusions

Airfoil self-noise or trailing edge noise was investigated experimentally using an open subsonic wind tunnel focusing on noise mechanisms at the trailing edge to identify and better understand sources of noise production which is essential in order to mitigate the acoustic scatter through better design of airfoils for various application in the aircraft and marine industry. The sound measurement profiles were captured by embedding microphones along the chord at various distances from the trailing edge and at different geometric angles of attack. The embedded microphones have successfully captured all noise sources due to aerodynamic flow over the NACA 0012 airfoil at the trailing edge, which included the following major peak frequencies 44 Hz, 93 Hz, 166 Hz and 332Hz. The fundamental frequency of the model tested was identified by peak frequency (166Hz). It appears that these frequencies do not deviate as the angle of attack is increased. The general trend is Strohal numbers decrease as the flow moves downstream which indicate the amount of resonance (i.e. periodic, non-random vortices) decreases further downstream, which is to be expected given the onset of turbulence. Two bands of frequencies were identified. The frequency spectra between 1 to 3kHz show a measure of far field noise energy while frequency spectra in the range 3 to 10kHz shows near field noise energy which is due to mechanisms associated with wake flow (separation).

Acknowledgments

The research was conducted by Beren R Jackson in partial fulfillment of BSc (Hons) in Aerospace Technology at the Department of Engineering and Math at Sheffield Hallam University under the supervision of Dr. Sam M Dakka.

References

[1] Brooks, T.F., Pope, D.S. and Marcolini, M.A., “Airfoil Self-Noise and Prediction,” Technical Report. NASA Reference Publication 1218, 1989, pp. 1-146

[2] Roger, M. and Moreau, S., “Broadband self-noise from loaded fan blades,” AIAA Journal, Vol. 42, No. 3, 2004, pp. 536-544

[3] Roger, M., Moreau, S., "Trailing Edge Noise Measurements and Prediction for Subsonic Loaded Fan Blades, AIAA Paper No. 2002-2460," 8th AIAA/CEAS Aeroacoustics Conference & Exhibit, Breckenridge, Colorado, 17-19 June 2002.

[4] FfowcsWilliams, J. and Hall, L., "Aerodynamic sound generation by turbulent flow in the vicinity of a scattering half-plane," Journal of Fluid Mechanics, Vol. 40, 1970, pp. 657–670.

[5] Amiet, R., "Noise due to turbulent flow past a trailing edge," Journal of Sound and Vibration Vol. 47, 1976, pp. 387–393.

[6] Howe, M., "A review of the theory of trailing edge noise," Journal of Sound and Vibration Vol. 61, 1978, pp. 437–465.

[7] Brooks, T.F. and Hodgson, T.H., "Trailing edge noise prediction from measured surface pressures," Journal of Sound and Vibration, Vol. 78, 1981, pp. 69–117.

[8] Brooks, T.F., Pope, D.S. and Marcolini, M.A., "Airfoil Self-Noise and Prediction," Technical Report. NASA Reference Publication 1218, 1989, pp. 1-146

[9] Farnell, *Pico Technology PicoScope Oscilloscope*, 2015, Leeds, UK: PicoTech, Available: http://uk.farnell.com/pico-technology/picoscope-3425/pc-oscilloscope-differential/dp/1670526

[10] Garcia-Sagrado, A. and Hynes, T., "*Wall Pressure Sources near an Airfoil Trailing Edge under Turbulent Boundary Layers*," Journal of Fluids and Structures, Vol. 30, 2012, pp. 3-34

[11] Lilley, G.M., "*The Prediction of Airframe Noise and Comparison with Experiment"*, Penn State University, University Park, PA, 2001: Academic Press.

[12] Brooks, T.F. and Hodgson, T.H., "Trailing edge noise prediction from measured surface pressures," Journal of Sound and Vibration, Vol. 78, 1981, pp. 69–117.

[13] Banks, C., "*Boundary Layer Parameters,"* 1999, America, Available: http://aerojockey.com/papers/bl/node2.html.

[14] Garcia-Sagrado, A. and Hynes, T. "*Stochastic estimation of flow near the trailing edge of a NACA0012 airfoil*," Experiments in Fluids: experimental methods and their applications to fluid flow, Vol. 51, 2011, pp. 1057-1071.

FIGURE CAPTIONS

Figure 1. Top view of NACA0012 final model, as tested in the wind tunnel.

Figure 2. Microphone location: The coordinate system indicated in table 7 has its origin at the leading edge-mid span of the airfoil.

Figure 3. Side view of the produced airfoil model.

List of Tables

Appendix 1

Reynolds Numbers (Re_x): $Re_x = \frac{V_\infty x}{v}$

$$(Microphone\ 10)\ Re_x = \frac{20 \times 0.272}{1.46 \times 10^{-5}} = \mathbf{372603}$$

Boundary Layer Thicknesses (δ): $\delta_{laminar} = \frac{5.2x}{\sqrt{Re_x}}$

$$(Microphone\ 10)\ \delta_{laminar} = \frac{5.2 \times 0.272}{\sqrt{372603}} = \mathbf{0.00232m}$$

Skin Friction Coefficients (Cf_x): $Cf_{x,laminar} = \frac{0.664}{\sqrt{Re_x}}$

$$(Microphone\ 10)\ Cf_{x,laminar} = \frac{0.664}{\sqrt{372603}} = \mathbf{0.00109}$$

$$Cf_{x,turbulent} = \frac{0.0592}{Re_x^{0.2}} \qquad (Microphone\ 10)\ Cf_{x,turbulent} = \frac{0.0592}{372603^{0.2}} = \mathbf{0.00455}$$

Wall Shear Stresses (τ_w): $\tau_w = \frac{1}{2}\rho_\infty V_\infty^2 \begin{bmatrix} Cf_{x,laminar} \\ Cf_{x,turbulent} \end{bmatrix}$

$$(Microphone\ 10)\ \tau_w = 225 \times \begin{bmatrix} 0.00109 \\ 0.00455 \end{bmatrix} = \begin{bmatrix} \mathbf{0.267Pa} \\ \mathbf{1.115Pa} \end{bmatrix}$$

Strouhal Numbers (S_t): $S_T = \frac{f_{peak} \sin\theta\, \bar{c}}{V_\infty}$

$$(Microphone\ 1, 16°\ AoA)\ S_T = \frac{527 \times \sin(90 - 16) \times 0.027}{20} = \mathbf{0.684}$$

Noise Intensity (I): $I = K\left(\frac{LV_\infty M_\infty^2}{\bar{C_L}}\right)$

$$(0°\ AoA)\ I = 7 \times 10^{-7}\left(\frac{3.129 \times 20 \times 0.059^2}{0.59586}\right) = \mathbf{0.2559\mu W/m^2}$$

Overall Acoustic Sound Pressure Level (OASPL):

$$OASPL(dB) = 120 + 10log_{10}I$$

$$(16°\ AoA)\ OASPL = 120 + 10log_{10}(0.9258 \times 10^{-6}) = \mathbf{59.67dB}$$

Knee Frequency Wavelengths (λ): $c = f\lambda$

$$(Microphone\ 10, 16°\ AoA)\ \lambda = \frac{2602}{340.29} = \mathbf{0.1308m}$$

Figures

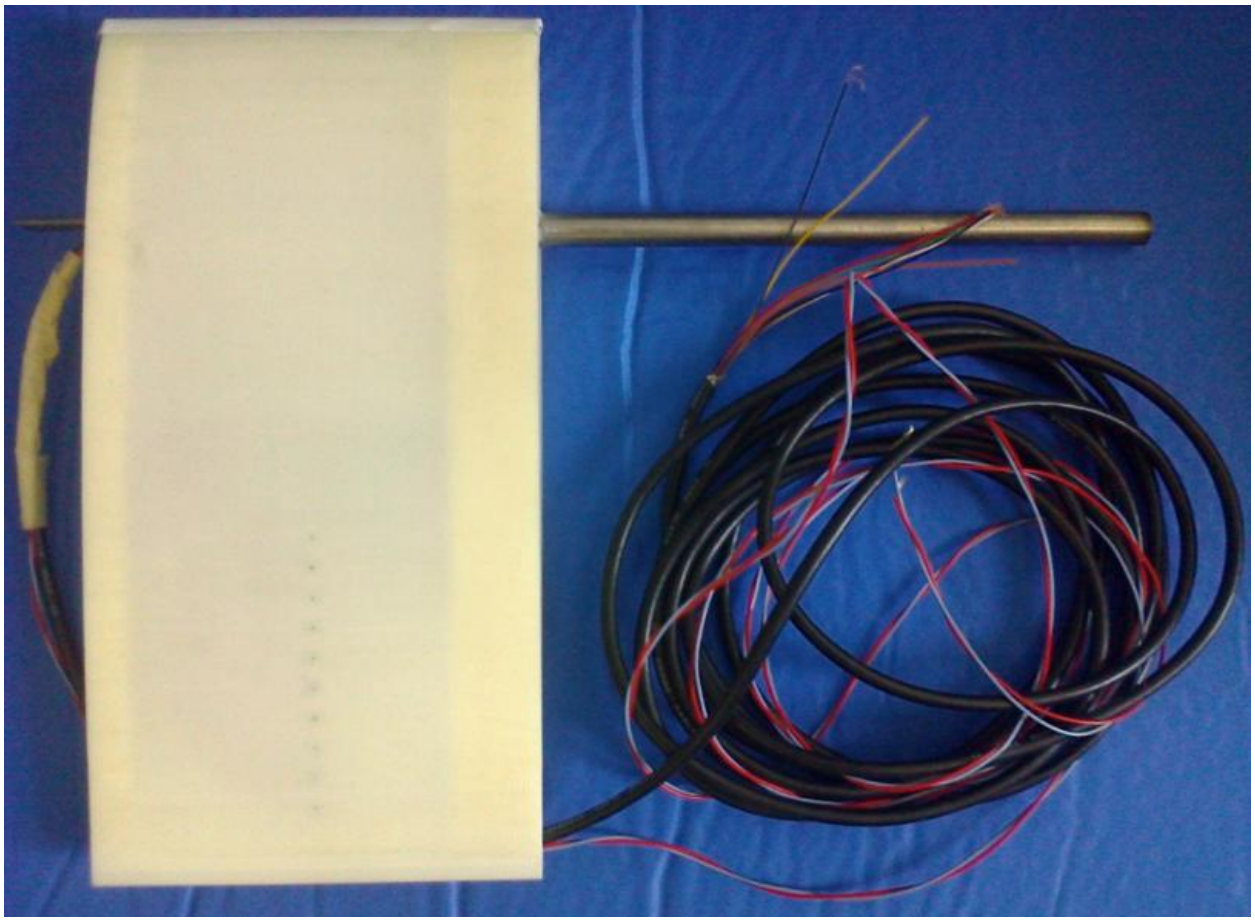

Figure 1: Top view of NACA0012 final model, as tested in the wind tunnel.

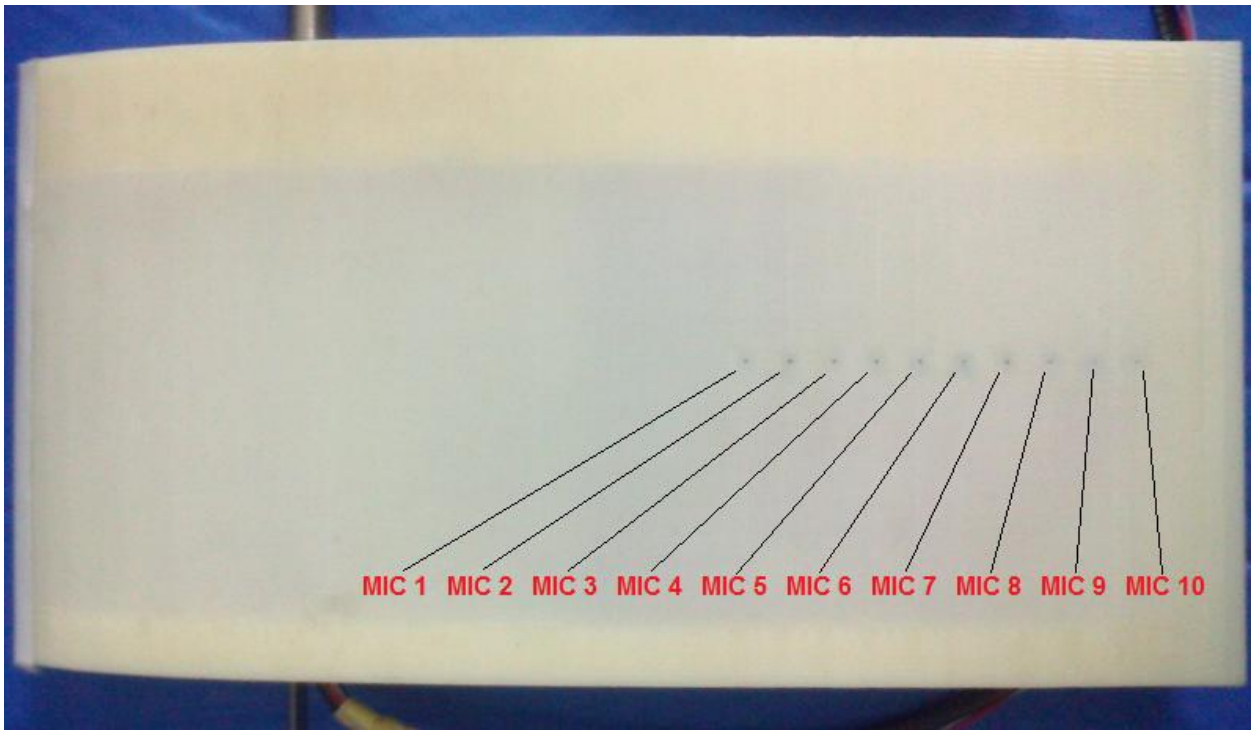

Fig 2. Microphone location: The coordinate system indicated in table 1 has its origin at the leading edge-mid span of the airfoil.

Fig 3. Side view of the produced airfoil model.

0° AoA:

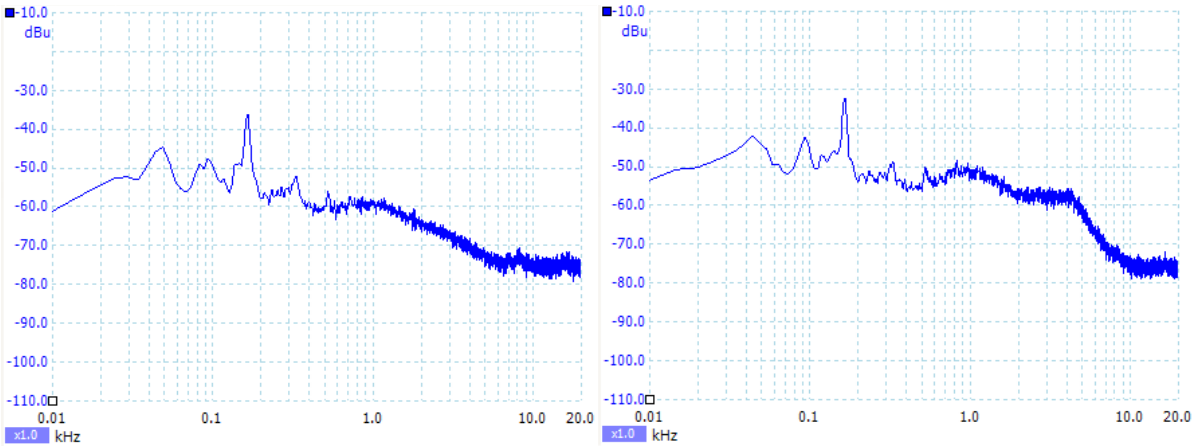

Fig.4. dBu vs Frequency, Microphone 1 **Fig.5.** dBu vs Frequency, Microphone 2

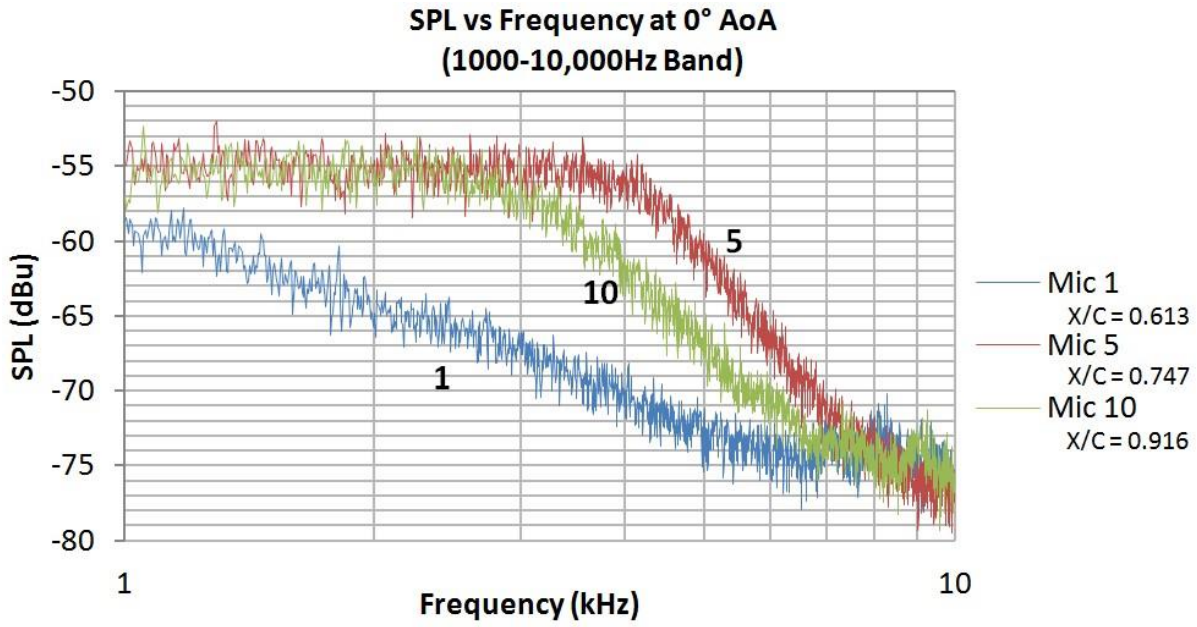

Fig.6. Frequency as a function of dBu at 0°.

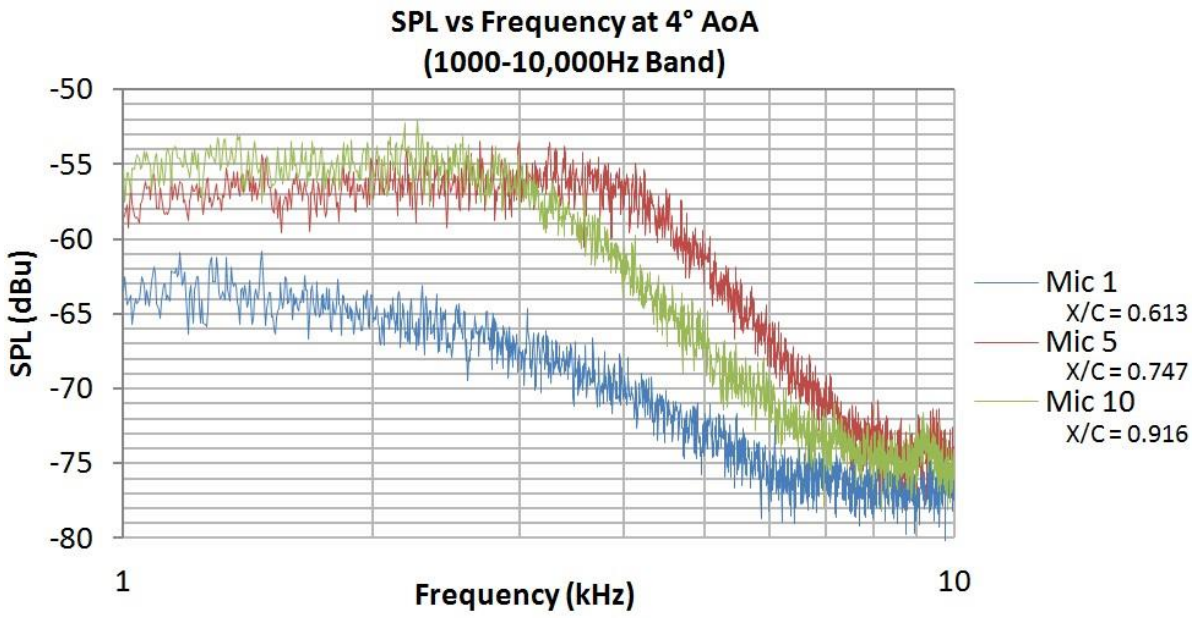

Fig7. Frequency as a function of dBu at 4°.

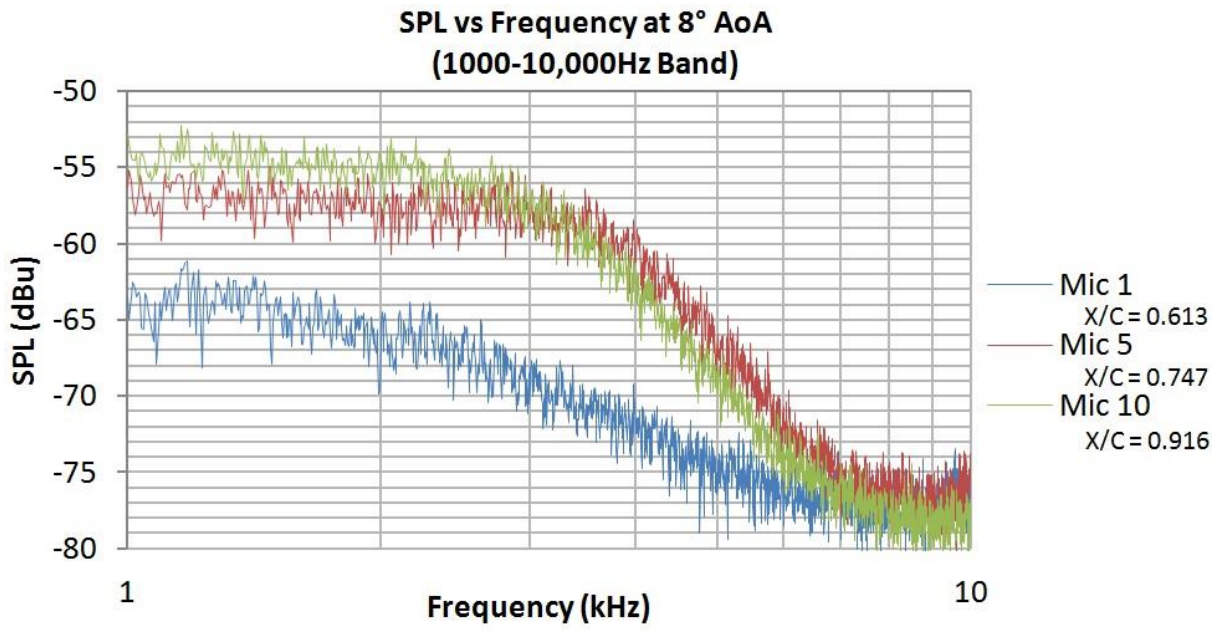

Fig.8. Frequency as a function of dBu at 8°.

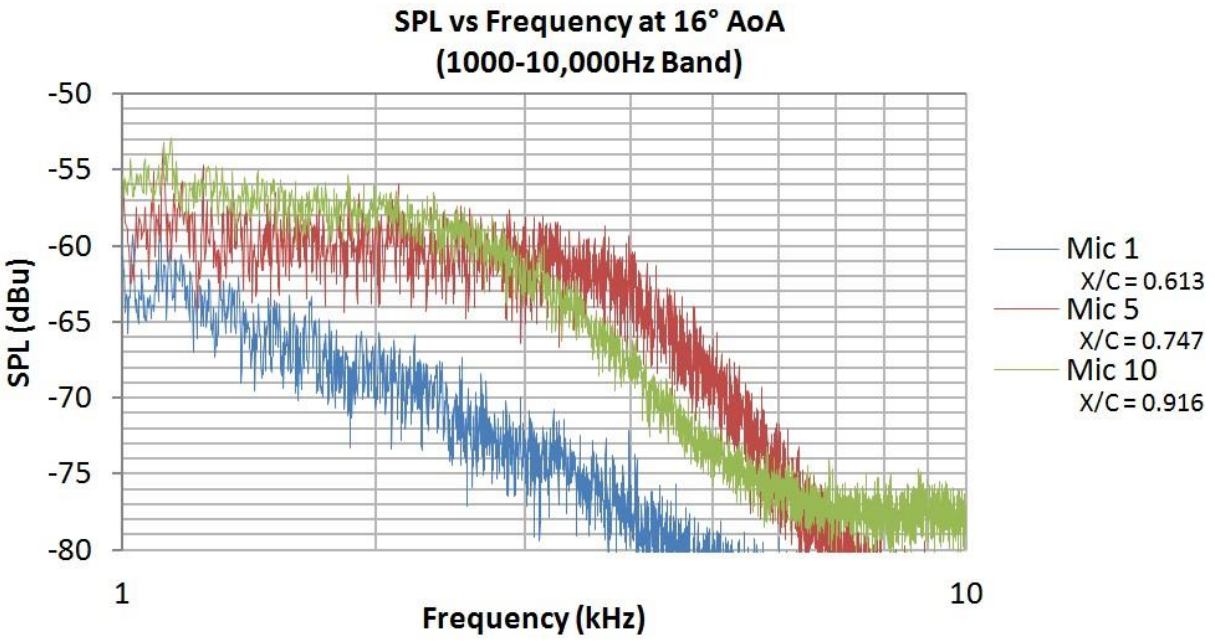

Fig.9. Frequency as a function of dBu at 16°.

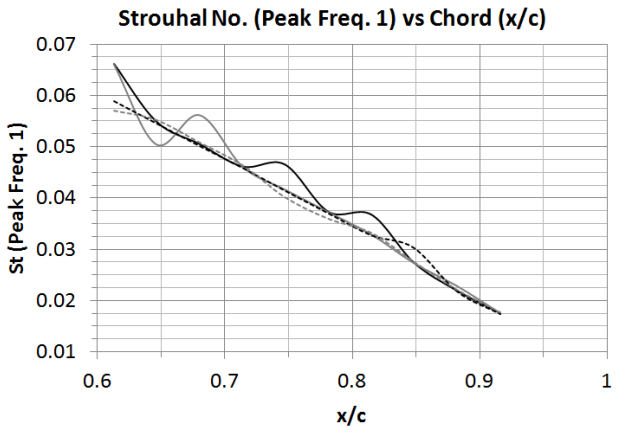
Strouhal No. (Peak Freq. 1) vs Chord (x/c)
St (Peak Freq. 1)
0.07
0.06
0.05
0.04
0.03
0.02
0.01
0.6
0.7
0.8
0.9
1
x/c

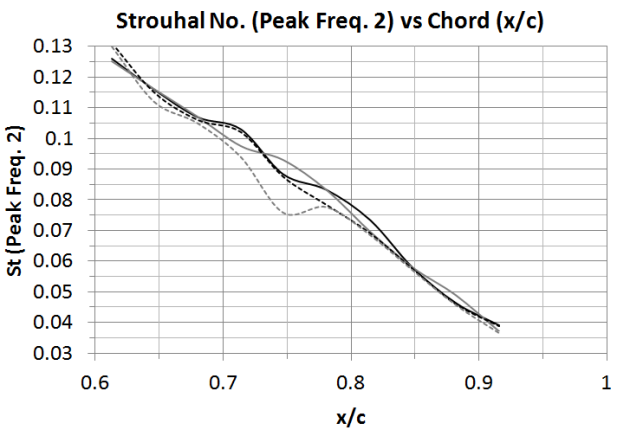
Strouhal No. (Peak Freq. 2) vs Chord (x/c)
St (Peak Freq. 2)
0.13
0.12
0.11
0.1
0.09
0.08
0.07
0.06
0.05
0.04
0.03
0.6
0.7
0.8
0.9
1
x/c

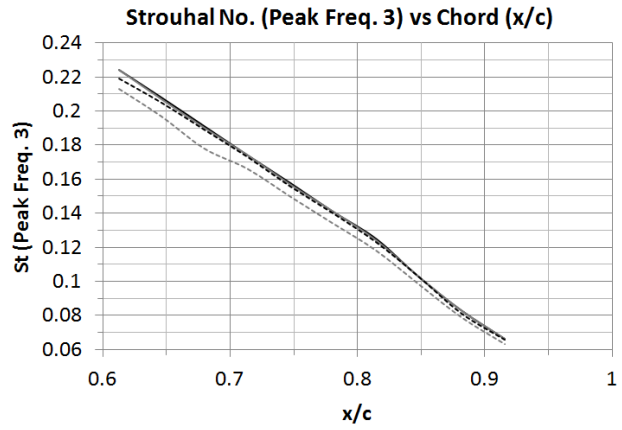
Strouhal No. (Peak Freq. 3) vs Chord (x/c)
St (Peak Freq. 3)
0.24
0.22
0.2
0.18
0.16
0.14
0.12
0.1
0.08
0.06
0.6
0.7
0.8
0.9
1
x/c

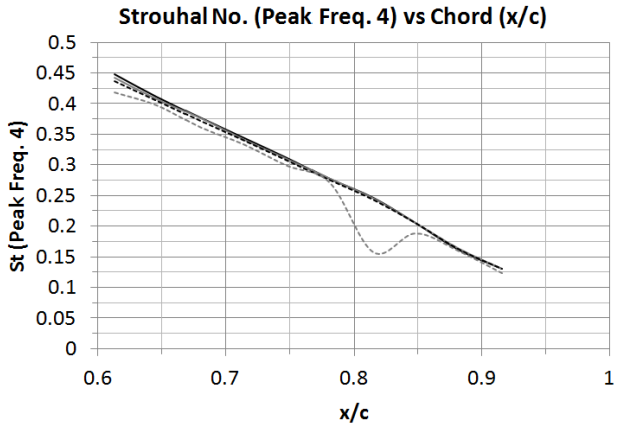
Strouhal No. (Peak Freq. 4) vs Chord (x/c)
St (Peak Freq. 4)
0.5
0.45
0.4
0.35
0.3
0.25
0.2
0.15
0.1
0.05
0
0.6
0.7
0.8
0.9
1
x/c

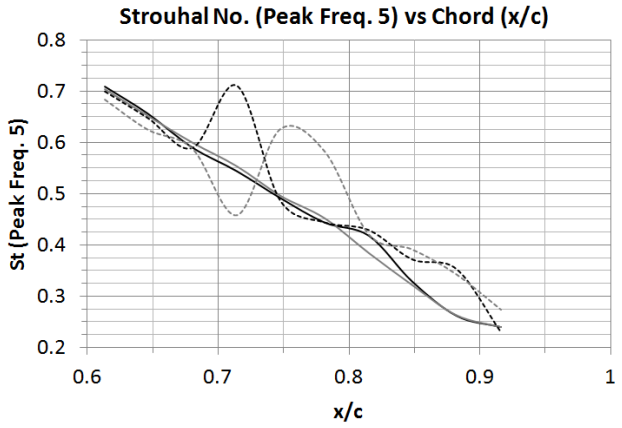
Strouhal No. (Peak Freq. 5) vs Chord (x/c)
St (Peak Freq. 5)
0.8
0.7
0.6
0.5
0.4
0.3
0.2
0.6
0.7
0.8
0.9
1
x/c

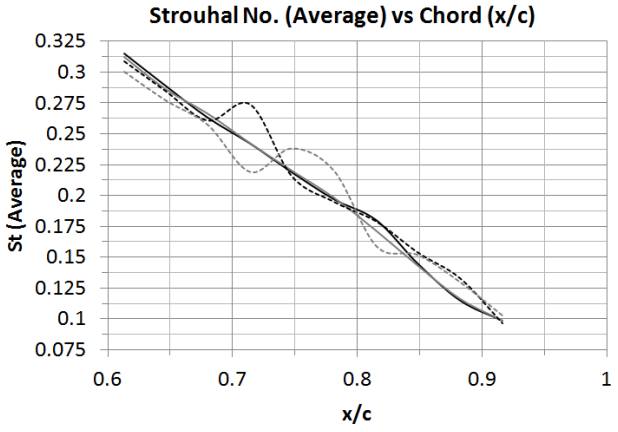
Strouhal No. (Average) vs Chord (x/c)
St (Average)
0.325
0.3
0.275
0.25
0.225
0.2
0.175
0.15
0.125
0.1
0.075
0.6
0.7
0.8
0.9
1
x/c

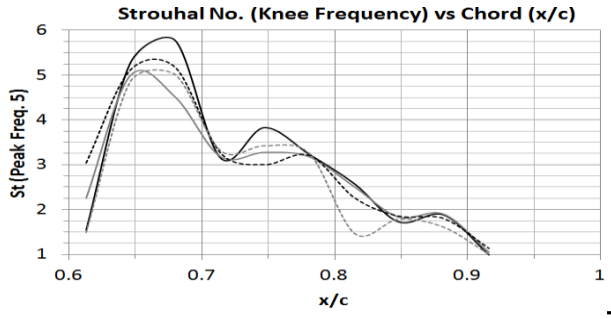
Strouhal No. (Knee Frequency) vs Chord (x/c)
St (Peak Freq. 5)
6
5
4
3
2
1
0.6
0.7
0.8
0.9
1
x/c

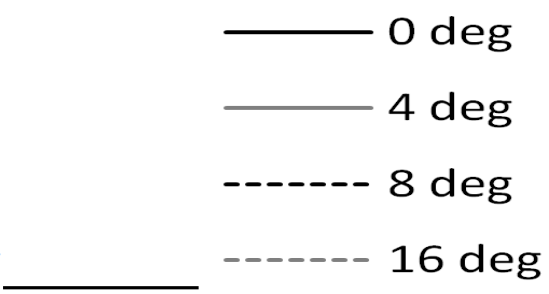
0 deg
4 deg
8 deg
16 deg

Fig.10. Strouhal Number at different peak frequencies versus chord length

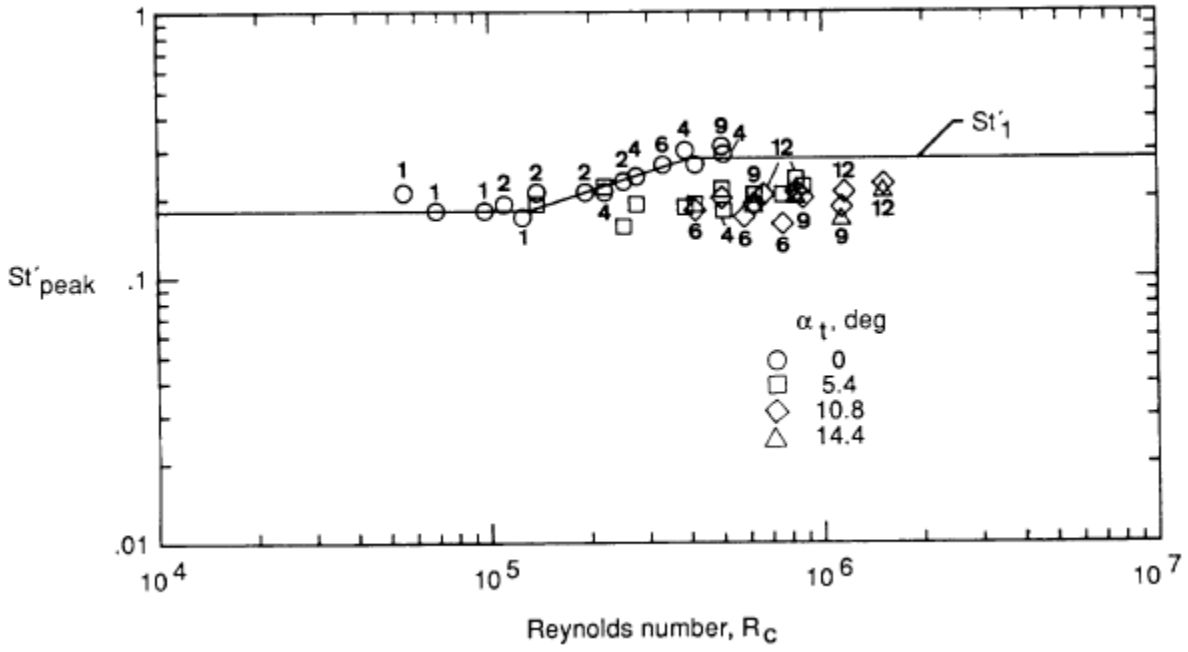

Fig.11. Laminar boundary layer (LBL) peak Strouhal numbers vs. Reynolds number. Numbers represent chord size in inches, (Brooks, Pope and Marcolini, 1989).

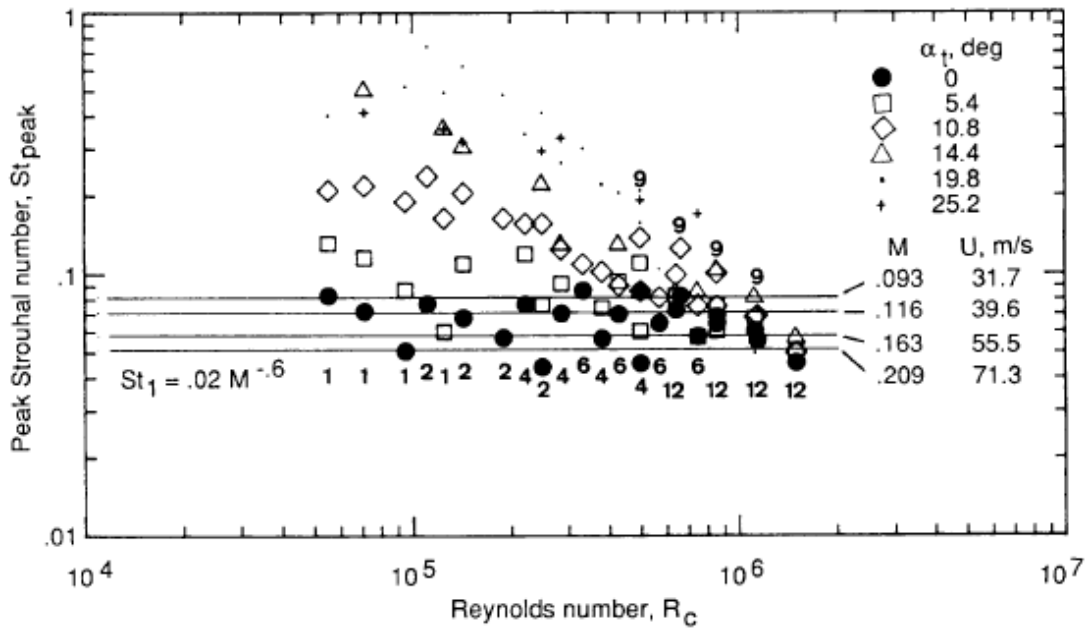

Fig.12. Turbulent boundary layer (TBL) peak Strouhal numbers vs. Reynolds number. Numbers represent chord size in inches,
(Brooks, Pope and Marcolini, 1989).

Table 1: Positions of each microphone in relation to airfoil chord length

Microphone No.	X/C	Distance from Leading Edge/mm	Distance from mid-span/mm
1	0.613	182	0
2	0.646	192	0
3	0.680	202	0
4	0.714	212	0
5	0.747	222	0
6	0.781	232	0
7	0.815	242	0
8	0.848	252	0
9	0.882	262	0
10	0.916	272	0

Table 2: Results of acoustic spectrum analysis for 0°

Mic No.	AoA (°)	Speed (m/s)	Mach No.	Free-stream Reynolds No.	Peak Freq. 1 (Hz)	Peak Freq. 2 (Hz)	Peak Freq. 3 (Hz)	Peak Freq. 4 (Hz)	Peak Freq. 5 (Hz)	Knee Freq. (Hz)	SPL at Knee (dBu)
1	0	20	0.059	406849	49	93	166	332	525	1140	-59.13
2	0	20	0.059	406849	44	93	166	329	525	4207	-57.4
3	0	20	0.059	406849	44	93	166	328	513	5022	-61.21
4	0	20	0.059	406849	44	98	166	328	518	3002	-58.1
5	0	20	0.059	406849	49	93	166	328	518	4028	-55.33
6	0	20	0.059	406849	44	98	166	326	522	3798	-54.98
7	0	20	0.059	406849	49	98	166	328	557	3427	-63.29
8	0	20	0.059	406849	44	93	165	328	526	2758	-54.64
9	0	20	0.059	406849	44	93	166	322	523	3751	-58.1
10	0	20	0.059	406849	44	98	166	326	600	2466	-54.64

Table 3: Results of acoustic spectrum analysis for 4°

Mic No.	AoA (°)	Speed (m/s)	Mach No.	Free-stream Reynolds No.	Peak Freq. 1 (Hz)	Peak Freq. 2 (Hz)	Peak Freq. 3 (Hz)	Peak Freq. 4 (Hz)	Peak Freq. 5 (Hz)	Knee Freq. (Hz)	SPL at Knee (dBu)
1	4	20	0.059	406849	49	93	166	328	522	1675	-63.63
2	4	20	0.059	406849	44	93	166	326	522	3997	-54.64
3	4	20	0.059	406849	49	93	166	328	522	3933	-59.13
4	4	20	0.059	406849	44	93	166	326	528	3040	-59.13
5	4	20	0.059	406849	44	98	166	327	523	3458	-55.67
6	4	20	0.059	406849	44	98	166	327	533	3747	-55.67
7	4	20	0.059	406849	44	93	166	327	513	3348	-62.6
8	4	20	0.059	406849	44	93	166	328	517	2943	-56.02
9	4	20	0.059	406849	49	98	166	327	528	3808	-58.44
10	4	20	0.059	406849	44	93	166	327	601	2630	-54.64

Table 4: Results of acoustic spectrum analysis for 8°

Mic No.	AoA (°)	Speed (m/s)	Mach No.	Free-stream Reynolds No.	Peak Freq. 1 (Hz)	Peak Freq. 2 (Hz)	Peak Freq. 3 (Hz)	Peak Freq. 4 (Hz)	Peak Freq. 5 (Hz)	Knee Freq. (Hz)	SPL at Knee (dBu)
1	8	20	0.059	406849	44	98	164	327	523	2275	-66.06
2	8	20	0.059	406849	44	93	166	327	523	4128	-55.67
3	8	20	0.059	406849	44	93	166	327	517	4546	-60.52
4	8	20	0.059	406849	44	98	166	327	683	3139	-60.17
5	8	20	0.059	406849	44	93	166	327	518	3190	-57.06
6	8	20	0.059	406849	44	93	166	327	527	3808	-57.06
7	8	20	0.059	406849	44	93	166	327	578	3040	-62.6
8	8	20	0.059	406849	49	93	166	332	601	2991	-56.71
9	8	20	0.059	406849	44	93	164	327	713	3629	-59.83
10	8	20	0.059	406849	44	98	166	327	581	2850	-56.02

Table 5: Results of acoustic spectrum analysis for 16°

Mic No.	AoA (°)	Speed (m/s)	Mach No.	Free-stream Reynolds No.	Peak Freq. 1 (Hz)	Peak Freq. 2 (Hz)	Peak Freq. 3 (Hz)	Peak Freq. 4 (Hz)	Peak Freq. 5 (Hz)	Knee Freq. (Hz)	SPL at Knee (dBu)
1	16	20	0.059	406849	44	100	164	322	527	1147	-61.9
2	16	20	0.059	406849	46	93	164	330	520	4036	-61.56
3	16	20	0.059	406849	46	95	161	327	532	4537	-66.75
4	16	20	0.059	406849	46	93	164	330	454	3288	-65.02
5	16	20	0.059	406849	44	83	164	327	686	3751	-61.56
6	16	20	0.059	406849	44	95	164	330	713	3977	-60.17
7	16	20	0.059	406849	46	95	164	218	582	2029	-61.56
8	16	20	0.059	406849	46	95	164	313	650	2968	-61.21
9	16	20	0.059	406849	46	95	164	330	711	3337	-61.9
10	16	20	0.059	406849	46	95	164	320	711	2602	-58.79

Table 6: Strouhal Numbers for peak frequencies at 0° AoA:

Mic No.	1	2	3	4	5	6	7	8	9	10
x/c	0.613	0.646	0.68	0.714	0.747	0.781	0.815	0.848	0.882	0.916
St, f1	0.0662	0.055	0.0506	0.0462	0.0466	0.0374	0.0368	0.0275	0.022	0.0176
St, f2	0.126	0.116	0.107	0.103	0.0884	0.0833	0.0735	0.0581	0.0465	0.0392
St, f3	0.224	0.208	0.191	0.174	0.158	0.141	0.125	0.103	0.083	0.0664
St, f4	0.448	0.411	0.377	0.344	0.312	0.277	0.246	0.205	0.161	0.13
St, f5	0.709	0.656	0.59	0.544	0.492	0.444	0.418	0.329	0.262	0.24
St Average	0.315	0.289	0.263	0.242	0.219	0.197	0.18	0.145	0.115	0.0986
St, Knee	1.539	5.259	5.775	3.152	3.827	3.228	2.57	1.724	1.876	0.986

Table 7: Strouhal Numbers for peak frequencies at 4° AoA:

Mic No.	1	2	3	4	5	6	7	8	9	10
x/c	0.613	0.646	0.68	0.714	0.747	0.781	0.815	0.848	0.882	0.916
St, f1	0.066	0.0505	0.0562	0.0461	0.0417	0.0373	0.0329	0.0274	0.0229	0.0176
St, f2	0.125	0.116	0.107	0.0974	0.0929	0.0831	0.0696	0.058	0.0489	0.0371
St, f3	0.224	0.207	0.19	0.174	0.157	0.141	0.124	0.103	0.0828	0.0662
St, f4	0.442	0.407	0.376	0.341	0.31	0.277	0.245	0.205	0.163	0.13
St, f5	0.703	0.651	0.599	0.553	0.496	0.452	0.384	0.322	0.263	0.24
St Average	0.312	0.286	0.266	0.242	0.22	0.198	0.171	0.143	0.116	0.0982
St, Knee	2.256	4.984	4.512	3.184	3.277	3.177	2.505	1.835	1.899	1.049

Table 8: Strouhal Numbers for peak frequencies at 8° AoA:

Mic No.	1	2	3	4	5	6	7	8	9	10
x/c	0.613	0.646	0.68	0.714	0.747	0.781	0.815	0.848	0.882	0.916
St, f1	0.0588	0.0545	0.0501	0.0458	0.0414	0.037	0.0327	0.0303	0.0218	0.0174
St, f2	0.131	0.115	0.106	0.102	0.0875	0.0783	0.0691	0.0576	0.046	0.0388
St, f3	0.219	0.205	0.189	0.173	0.156	0.14	0.123	0.103	0.0812	0.0658
St, f4	0.437	0.405	0.372	0.34	0.308	0.275	0.243	0.205	0.162	0.13
St, f5	0.699	0.647	0.589	0.71	0.487	0.444	0.429	0.372	0.353	0.23
St Average	0.309	0.285	0.261	0.274	0.216	0.195	0.179	0.154	0.133	0.0964
St, Knee	3.041	5.11	5.177	3.264	3.001	3.205	2.258	1.851	1.797	1.129

Table 9: Strouhal Numbers for peak frequencies at 16° AoA:

Mic No.	1	2	3	4	5	6	7	8	9	10
x/c	0.613	0.646	0.68	0.714	0.747	0.781	0.815	0.848	0.882	0.916
St, f1	0.0571	0.0553	0.0509	0.0464	0.0402	0.036	0.0332	0.0276	0.0221	0.0177
St, f2	0.13	0.112	0.105	0.0939	0.0758	0.0776	0.0685	0.0571	0.0457	0.0365
St, f3	0.213	0.197	0.178	0.166	0.15	0.134	0.118	0.0985	0.0788	0.0631
St, f4	0.418	0.397	0.361	0.333	0.299	0.27	0.157	0.188	0.159	0.123
St, f5	0.684	0.625	0.588	0.458	0.626	0.583	0.42	0.391	0.342	0.273
St Average	0.3	0.277	0.257	0.219	0.238	0.22	0.159	0.152	0.13	0.103
St, Knee	1.488	4.85	5.015	3.319	3.425	3.249	1.463	1.783	1.604	1

Table 10: Trailing edge boundary layer parameters for a NACA 0012 at 0° AoA, (Brooks and Hodgson, 1981)

U_0(m/s)	U_1(m/s)	c_f	u^*(m/s)	δ^*(cm)	Θ(cm)	δ^*(cm) best fit
23·2	21·3	0·00225	0·7064	0·4274	0·2748	0·4125
38·6	35·9	0·00215	1·1623	0·4003	0·2641	0·4082
46·3	43·3	0·00200	1·3533	0·4063	0·2702	0·4063
54·1	50·8	0·00200	1·5855	0·4089	0·2730	0·4030
61·8	58·2	0·00200	1·8169	0·4005	0·2678	0·4013

Table 11: Surface parameters dependent on chord-wise location (level-flight):

Airfoil Location	x/c	Re (x)	Laminar δ (mm)	Turbulent δ (mm)	Laminar Cfx ($x10^{-3}$)	Turbulent Cfx ($x10^{-3}$)	Laminar Wall Shear Stress Tw (Pa)	Turbulent Wall Shear Stress Tw (Pa)
10%	0.1	40685	0.766	1.32	3.29	7.09	0.806	1.737
20%	0.2	81370	1.08	2.29	2.33	6.17	0.571	1.512
30%	0.3	122055	1.33	3.17	1.9	5.69	0.466	1.394
40%	0.4	162740	1.53	3.99	1.65	5.37	0.404	1.316
50%	0.5	203425	1.71	4.77	1.47	5.14	0.36	1.259
60%	0.6	244110	1.88	5.52	1.34	4.95	0.328	1.213
Mic 1	0.613	249315	1.9	5.61	1.33	4.93	0.326	1.208
Mic 2	0.646	263014	1.95	5.85	1.29	4.88	0.316	1.196
Mic 3	0.68	276712	2	6.1	1.26	4.83	0.309	1.183
Mic 4	0.714	290411	2.05	6.34	1.23	4.78	0.301	1.171
Mic 5	0.747	304110	2.09	6.58	1.2	4.74	0.294	1.161
Mic 6	0.781	317808	2.14	6.81	1.18	4.7	0.289	1.152
Mic 7	0.815	331507	2.19	7.05	1.15	4.66	0.282	1.142
Mic 8	0.848	345205	2.23	7.28	1.13	4.62	0.277	1.132
Mic 9	0.882	358904	2.27	7.51	1.11	4.58	0.272	1.122
Mic 10	0.916	372603	2.32	7.74	1.09	4.55	0.267	1.115
Full Chord	1	406849	2.42	8.3	1.04	4.47	0.255	1.095

Table 12: Wavelengths of microphone knee frequency at each AoA:

Mic. No.	0° Knee Freq. (Hz)	λ (m)	λ (mm)	4° Knee Freq. (Hz)	λ (m)	λ (mm)	8° Knee Freq. (Hz)	λ (m)	λ (mm)	16° Knee Freq. (Hz)	λ (m)	λ (mm)
1	1140	0.2985	298.5	1675	0.2032	203.2	2275	0.1496	149.6	1147	0.2967	296.7
2	4207	0.0809	80.9	3997	0.0851	85.1	4128	0.0824	82.4	4036	0.0843	84.3
3	5022	0.0678	67.8	3933	0.0865	86.5	4546	0.0749	74.9	4537	0.075	75
4	3002	0.1134	113.4	3040	0.1119	111.9	3139	0.1084	108.4	3288	0.1035	103.5
5	4028	0.0845	84.5	3458	0.0984	98.4	3190	0.1067	106.7	3751	0.0907	90.7
6	3798	0.0896	89.6	3747	0.0908	90.8	3808	0.0894	89.4	3977	0.0856	85.6
7	3427	0.0993	99.3	3348	0.1016	101.6	3040	0.1119	111.9	2029	0.1677	167.7
8	2758	0.1234	123.4	2943	0.1156	115.6	2991	0.1138	113.8	2968	0.1147	114.7
9	3751	0.0907	90.7	3808	0.0894	89.4	3629	0.0938	93.8	3337	0.102	102
10	2466	0.138	138	2630	0.1294	129.4	2850	0.1194	119.4	2602	0.1308	130.8

Table 13: Noise Intensity and OASPL with comparison of the average knee noise level:

AoA (°)	Noise Intensity ($\mu W/m^2$)	OASPL (dB)	Average Knee Level (-dBu)
0	0.2559	54.08	57.682
4	0.3296	55.18	57.957
8	0.5406	57.33	59.17
12	0.8514	59.3	N/A
16	0.9258	59.67	62.04

Table 14: Chord length points (X) and trailing edge thicknesses:

Microphone	X /m (x/c)	TE Thickness ( ) /m
1	0.182 (0.613)	0.027
2	0.192 (0.646)	0.025
3	0.202 (0.680)	0.023
4	0.212 (0.714)	0.021
5	0.222 (0.747)	0.019
6	0.232 (0.781)	0.017
7	0.242 (0.815)	0.015
8	0.252 (0.848)	0.0125
9	0.262 (0.882)	0.010
10	0.272 (0.916)	0.008